

Soft Matter

Accepted Manuscript



This is an *Accepted Manuscript*, which has been through the Royal Society of Chemistry peer review process and has been accepted for publication.

Accepted Manuscripts are published online shortly after acceptance, before technical editing, formatting and proof reading. Using this free service, authors can make their results available to the community, in citable form, before we publish the edited article. We will replace this *Accepted Manuscript* with the edited and formatted *Advance Article* as soon as it is available.

You can find more information about *Accepted Manuscripts* in the [Information for Authors](#).

Please note that technical editing may introduce minor changes to the text and/or graphics, which may alter content. The journal's standard [Terms & Conditions](#) and the [Ethical guidelines](#) still apply. In no event shall the Royal Society of Chemistry be held responsible for any errors or omissions in this *Accepted Manuscript* or any consequences arising from the use of any information it contains.

Calculating Pressure in Polymer Lattice Simulations

Pengfei Zhang and Qiang Wang*

Department of Chemical and Biological Engineering

Colorado State University

Fort Collins, CO 80523-1370

October 29, 2014

Abstract

We proposed several novel methods for calculating the bulk pressure in polymer lattice simulations. Our first method combines chain insertion/deletion with Wang-Landau – Optimized Ensemble sampling in the space of number of chains n , which is very efficient and accurate at low to intermediate polymer volume fractions ϕ (e.g., $\lesssim 0.7$). We then proposed two methods in canonical-ensemble simulations to efficiently and accurately calculate the bulk pressure at high ϕ where chain insertion/deletion become inefficient. Finally, combining these methods leads to complete thermodynamics over the *entire* range of continuous and exact ϕ -values with negli-

*E-mail: q.wang@colostate.edu.

gible finite-size effects. We also analyzed in detail the error caused by the cut-off in n -space.

1 Introduction

Lattice Monte Carlo (MC) simulations are in general much faster than those in continuum and thus widely used in the study of polymeric systems. Calculating pressure in such simulations, however, is not trivial as the mechanical (virial) route commonly used in continuum is not applicable. In particular, this problem is the most severe at high densities (polymer volume fractions) ϕ , such as in concentrated polymer solutions or melts, where chain insertion/deletion cannot be performed efficiently due to their low acceptance rates, even with the configurational-bias Monte Carlo technique;¹ all methods for pressure calculation using chain insertion/deletion²⁻⁷ are therefore inefficient at such high ϕ , where the agreement between theories and simulations (thus our understanding) is also the worst.

Four classes of methods have been proposed in the literature. In the rest of this Section we give a brief overview of these methods, taking the commonly studied incompressible polymer solution as an example, where each lattice site is occupied by a total of ρ_0 polymer segments and solvent molecules having the same volume ($\rho_0 = 1$ corresponds to the conventional lattice model with the self- and mutual-avoiding walk). Throughout this work we take the lattice spacing and $k_B T$ as the unit of length and energy, respectively, where k_B denotes the Boltzmann constant and T the thermodynamic temperature.

1.1 Methods based on Grand-Canonical Partition Function

The test-chain insertion thermodynamic integration (μ TI) method² is based on the estimation of chain chemical potential $\mu \equiv (\partial F / \partial n)_V$ in canonical-ensemble (nVT) simulations

of n chains in volume V , which then gives $F(\phi, V) - F(\phi = 0, V) = (\rho_0 V/N) \int_0^\phi \mu d\phi$; here F denotes the system Helmholtz free energy, $\phi \equiv nN/\rho_0 V$ the polymer volume fraction, and N the number of segments on each chain. Since the pressure $P \equiv -(\partial F/\partial V)_n$, one then obtains the osmotic pressure $\Pi(\phi) = P(\phi) - P(\phi = 0) = (\rho_0/N) \left[\phi \mu(\phi) - \int_0^\phi \mu d\phi \right] = (\rho_0/N) \int_{\mu(\phi=0)}^{\mu(\phi)} \phi d\mu$, where the first integral has been evaluated numerically in either nVT^2 or grand-canonical-ensemble (μVT)⁵ simulations (with ϕ being the ensemble-averaged polymer volume fraction in the latter).

The compressibility route (denoted by κ_T TI), on the other hand, uses integration of the isothermal compressibility $\kappa_T \equiv -(\partial V/\partial P)_n/V = (\partial \phi/\partial P)_n/\phi$, leading to $\Pi(\phi) = \int_0^\phi (1/\kappa_T \phi) d\phi$, which has been used in both μVT^3 and nVT^8 simulations (with κ_T approximated from the total structure factor at small wave-vector lengths in the latter). Since $\kappa_T = (N/\rho_0 \phi^2)(\partial \phi/\partial \mu)_V$ and $\phi = (N/\rho_0 V)(\partial \ln \Xi/\partial \mu)_V$ in a grand-canonical ensemble, where Ξ denotes its partition function, we have $\Pi(\phi) = (\rho_0/N) \int_{\mu(\phi=0)}^{\mu(\phi)} \phi d\mu = \ln[\Xi(\mu(\phi), V)/\Xi_0]/V$ with $\Xi_0 \equiv \Xi(\mu(\phi = 0), V)$. The first equality shows the equivalence of μ TI and κ_T TI methods, and the second shows that both methods are actually based on estimating Ξ . Indeed, the computationally expensive numerical integration in both methods can be avoided if $\Xi(\mu(\phi), V)/\Xi_0$ is directly estimated; this was basically how Jiang and Wang⁴ calculated Π using many μVT simulations at different μ combined with the self-consistent histogram-reweighting technique.⁹

1.2 Methods based on Canonical Partition Function

The second class of methods are based on estimating the canonical partition function Z . In particular, the repulsive wall method (RWM) in nVT simulations proposed by Dickman¹⁰ calculates, by design, the normal pressure P_n of a *confined* film of lateral area A (under the periodic boundary conditions) and thickness D between two impenetrable walls placed (without loss of generality) at $x = 0$ and $D + 1$, respectively,

$$P_n(L_x) \approx \frac{1}{A} \ln \frac{Z(L_x)}{Z(L_x - 1)} \quad (1)$$

$$\begin{aligned} &= \frac{1}{A} \ln \frac{Z'(\lambda = 1)}{Z'(\lambda = 0)} - \ln(\rho_0!) \\ &= \frac{1}{A} \int_0^1 d\lambda \frac{\langle N_c \rangle_\lambda}{\lambda} - \ln(\rho_0!), \end{aligned} \quad (2)$$

where

$$Z = \frac{1}{n!} \sum_{\mathbf{R}} \frac{\exp[-H(\mathbf{R})]}{W(\mathbf{R})} \quad (3)$$

is the canonical partition function of the confined incompressible polymer solution, \mathbf{R} denotes a configuration of all chains, H is the system Hamiltonian due to both chain connectivity and non-bonded interactions (including the incompressibility constraint), $W = \prod_{\mathbf{r}} [\rho_0 - \rho(\mathbf{r})]!$ with $\rho(\mathbf{r})$ being the number of polymer segments at lattice site \mathbf{r} in \mathbf{R} ,¹¹ $Z'(\lambda) = (1/n!) \sum_{\mathbf{R}} \exp[-H(\mathbf{R})] \lambda^{N_c(\mathbf{R})} / W(\mathbf{R})$ is the canonical partition function of the same confined system but with a repulsive potential $U_c = -\ln \lambda$ acting on each segment at $x = L_x$ (i.e., the repulsive wall) and the contact number N_c being the total number of such segments, and $\langle \rangle_\lambda$ is the ensemble average given by $Z'(\lambda)$. To avoid the expensive numerical integration over the coupling parameter λ , Jimenez and Rajagopalan combined this method with Bennet's acceptance-ratio method,¹² and we recently combined it with Wang-Landau – Optimized Ensemble (WL-OE) sampling¹³

to estimate the density of states of N_c and also replaced the first-order backward finite difference in Eq. (1) by the second-order centered finite difference for higher accuracy.¹⁴

nVT simulations avoid chain insertion/deletion and can therefore be used to calculate pressure at high ϕ . When RWM is used to calculate the *bulk* pressure P in nVT simulations,¹⁰ however, the system is confined between two impenetrable surfaces and $P_n(L_x) = P(\phi_m)$ is assumed, where ϕ_m is taken as the polymer volume fraction in the middle of the confined film and has some statistical error due to the system fluctuations (note that, at high ϕ , small variation in ϕ leads to large change in P ; see Fig. 8 below). What is more problematic is that, due to the confinement effects of the walls, large L_x is required for ϕ_m to be close to the corresponding bulk value at the same μ as in the confined film.³ Indeed, Stukan et al. showed that the pressure correction due to the confinement effects is inversely proportional to L_x and is visible even at $L_x = 160$ (for a chain length of $N = 20$ and an average polymer volume fraction of 0.5) in nVT simulations.³ While they also showed that the confinement effects are much smaller if RWM is used in μVT simulations,³ this unfortunately limits its applicability to high ϕ .

1.3 Constant-Pressure (or Volume-Changing) Methods

The third class of methods uses MC trial moves to change V at given P . Nies and Cifra performed isothermal-isobaric-ensemble (nPT) simulations of polymer solutions confined between two impenetrable walls, one of which was built/destroyed by one lattice site in each trial move to change V occupied by the solution.¹⁵ Similar to RWM,¹⁰ this method has confinement effects when used for bulk systems. Such confinement effects are avoided

by Mackie et al., who inserted/deleted a randomly selected lattice layer of a bulk solution in each trial move by cutting all chains that cross the layer and then regrowing them.^{6,7} Since the acceptance rates of such trial moves would normally be very low, they used configurational bias¹ in their nPT ⁶ and Gibbs-ensemble⁷ simulations, with a high coordination number lattice, BFM3,¹⁶ also used in their Gibbs-ensemble simulations to further increase the acceptance rates. Similar to other methods using chain insertion/deletion,²⁻⁵ however, their method cannot be used at high ϕ where such trial moves cannot be performed efficiently.

1.4 The Hydrostatic Equilibrium Method

Finally, based on the local density approximation (LDA),¹⁷ Addison et al.¹⁸ proposed the hydrostatic equilibrium method (HEM) in nVT simulations. Here the system is confined between two walls as in RWM and is subject to a slowly varying external field $U(x) = \lambda x$ with the dimensionless parameter $\lambda > 0$. LDA then gives $dP/dx = -\lambda\rho_0\phi(x)$, and one can obtain $\Pi(x)$ by choosing x_0 to be large enough such that $\phi(x_0) = 0$.¹⁸ This method has the distinct advantage that Π over a range of ϕ can be obtained in a single simulation run, but its use of $U(x)$ requires large D and has certain limitations as examined by Ivanov et al.,⁵ they compared μ TI method in μVT simulations, RWM in both nVT and μVT simulations, and HEM for bulk pressure calculation, and concluded that HEM is far more efficient than RWM but comparable to the μ TI method.⁵

In this work we propose several novel methods that lead to efficient and accurate calculations of bulk pressure in lattice MC simulations over the *entire* range of ϕ . These

methods are described in Sec. 2, and their performance are reported in Sec. 3. Sec. 4 is devoted to summary.

2 Our Methods

2.1 The Z Method

We first introduce a method combining chain insertion/deletion with WL-OE sampling¹³ in n -space to calculate the bulk pressure, which not only avoids the expensive numerical integration required in μ TI method and the large system size required in HEM, but also has the same advantage as HEM, thus much more efficient than *all* the existing methods.^{2–8,10,15,18} This method is based on the direct estimation of the canonical partition function $Z(n, V)$ of a bulk system (given by Eq. (3)) for a range of n in a single simulation, thus referred to as the Z method here. Since $P(\mu)V = \ln \sum_{n=0}^{n_m} \exp(\mu n) Z(n, V)$ with the maximum number of chains in the system $n_m \rightarrow \infty$ in the thermodynamic limit, we then have

$$\Pi(\mu) = \frac{1}{V} \ln \sum_{n=0}^{n_m} \exp(\mu n) z(n, V) \quad (4)$$

with $z(n, V) \equiv Z(n, V)/Z_0$ and $Z_0 \equiv Z(n=0, V) = (\rho_0!)^{-V}$. On the other hand, with

$$\phi(\mu) = \frac{N}{\rho_0 V} \frac{\sum_{n=0}^{n_m} n \exp(\mu n) z(n, V)}{\sum_{n=0}^{n_m} \exp(\mu n) z(n, V)}, \quad (5)$$

$\Pi(\phi)$ is finally obtained over a range of ϕ . We note that the direct estimation of $Z(n, V)$ for a range of n using WL sampling was proposed by Ganzenmüllera and Camp, who applied it to determine the phase equilibrium of complex small molecules in continuum (off-lattice) simulations.¹⁹ Our use of WL-OE sampling overcomes the error saturation problem of WL sampling²⁰ and greatly improves the sampling efficiency and accuracy.¹³

2.1.1 Wang-Landau – Optimized Ensemble (WL-OE) Sampling

For given N , ρ_0 and V , our WL-OE sampling consists of two parts: first WL sampling is used to estimate Z crudely, then OE sampling to estimate Z accurately. At the beginning of WL sampling, an array $g(n)$ is set to unity and a histogram $h(n)$, which records the number of visits to any configuration having n chains (referred to as the “ n -state”) in the simulation, is set to 0 for all $n \in [0, n_m]$. We use two types of trial moves in our simulations. The first is nVT trial moves of random segment hopping and chain reptation with probabilities of 0.2 and 0.8, respectively, which keep n unchanged and have the acceptance criterion

$$\mathcal{P}_{acc}(\mathbf{R} \rightarrow \mathbf{R}') = \min \left[1, \frac{W}{W'} \exp(-\Delta H) \right] \quad (6)$$

with ΔH being the difference in H between the trial configuration \mathbf{R}' (having W') and the current configuration \mathbf{R} (having W). The second is chain insertion and deletion, which change n . Here the chain insertion and deletion are randomly chosen with equal probability and the configurational bias¹ is used. The acceptance criterion for inserting one chain into \mathbf{R} (having n chains) to generate \mathbf{R}' is

$$\mathcal{P}_{acc}(n \rightarrow n+1) = \min \left[1, \frac{Vg(n)W \exp(-\Delta H) R_i z_L^{N-1}}{(n+1)g(n+1)W'} \right] \quad (7)$$

if $n < n_m$ and 0 otherwise,²¹ where R_i is the Rosenbluth weight of the inserted chain and z_L the lattice coordination number, and that for deleting one chain from \mathbf{R} to generate \mathbf{R}' is

$$\mathcal{P}_{acc}(n \rightarrow n-1) = \min \left[1, \frac{ng(n)W \exp(-\Delta H)}{Vg(n-1)W' R_d z_L^{N-1}} \right], \quad (8)$$

where R_d is the Rosenbluth weight of the deleted chain. Note that for simplicity we are limited here to lattice models with all bonds having the same *a priori* probability,¹⁶

but it is straightforward to generalize our method to other lattice models.¹⁶ After each trial move, $g(n)$ and $h(n)$ of the current state (i.e., \mathbf{R}' if the trial move is accepted and \mathbf{R} otherwise) are updated according to $\ln g(n) \rightarrow \ln g(n) + \ln f$ and $h(n) \rightarrow h(n) + 1$, respectively, where f is a modification factor with an initial value of $f_0 = e \approx 2.718$. The histogram flatness, i.e., $h(n) > 0.8 \sum_{m=0}^{n_m} h(m)/(n_m + 1)$ for all n , is checked every 1000 Monte Carlo steps (MCS); here one MCS is defined as $n_m N nVT$ trial moves and n_m chain insertion/deletion trial moves. If the histogram is flat, we reset $h(n) = 0$ for all n and decrease f according to $f \rightarrow \sqrt{f}$. Once $f < 1.00001$, we stop WL sampling and switch to OE sampling¹³ to improve the accuracy of $g(n)$.

We start OE sampling with $g_1(n) = g(n)$ obtained from the above WL sampling. In addition, we use two arrays $h(n)$ and $h^+(n)$ with initial values of zero for all n , where $h(n)$ is used as above, and $h^+(n)$ for the number of visits to the n -state with the most recently visited extreme state being $n = 0$. The same acceptance criteria as given by Eqs. (6)~(8) are used. After each trial move, we only update the histogram of the current state as $h(n) \rightarrow h(n) + 1$; if the most recently visited extreme state is 0, we also update $h^+(n) \rightarrow h^+(n) + 1$. After 50 round-trips, where one round-trip is defined as the system reaching from the extreme state $n = 0$ to the other extreme state $n = n_m$ and then back to $n = 0$, we update $g(n)$ for all n as $g_{j+1}(n) = g_j(n) / \sqrt{[d\tilde{h}_j(n)/dn]/h_j(n)}$, where j denotes the simulation step using $g_j(n)$, $\tilde{h}_j(n) \equiv h_j^+(n)/h_j(n)$, and $d\tilde{h}_j(n)/dn$ is calculated using the second-order finite difference with the smallest step size in n that yields a positive value. We then increase the required number of round-trips in the simulation step by 1.3 times, reset $h(n)$ and $h^+(n)$ to 0 for all n , and continue the simulation with $g_{j+1}(n)$. At the end of simulation step j , $\ln Z(n, V)$ is estimated as

$\ln Z_j(n) = \ln Z_0 + \ln[h_j(n)/h_j(n=0)] + \ln[g_j(n)/g_j(n=0)]$. OE sampling is stopped when

$$\sqrt{\sum_{n=1}^{n_m} \left[\ln \frac{Z_{j+1}(n)}{Z_j(n)} \right]^2} / n_m < 0.05 \quad (9)$$

is satisfied. Finally, we estimate the error bar reported in our results below as the standard deviation calculated from three independent WL-OE simulations.

2.2 Two Variants of RWM in nVT Simulations

We then propose two variants of RWM in nVT simulations to efficiently calculate P at high ϕ , which not only avoid the confinement effects and the numerical integration over λ in Eq. (2), but also greatly improve the accuracy of the calculated $P(\phi)$. For a *bulk* system (i.e., without the two confining walls but with the periodic boundary conditions also in the x -direction), the right-hand-side of Eq. (1) gives the bulk pressure $P(\phi)$ with $\phi = nN/\rho_0 A(L_x - 1/2)$ via the *second*-order centered finite difference, and Eq. (3) now gives the canonical partition function of the bulk system; this is the starting point of our variants. For simplicity, we limit our discussion here to the square lattice in 2D and the simple cubic lattice in 3D, but it is straightforward to generalize our variants to other lattice models.¹⁶

2.2.1 The Repulsive Plane with Bridging Bonds (RPBB) Method

While the original RWM uses the repulsive wall to bridge two *confined* systems having L_x and $L_x - 1$ lattice layers in the x -direction, the first variant we propose is to use a repulsive plane with bridging bonds (RPBB) to bridge two *bulk* systems described by $Z(L_x)$ and $Z(L_x - 1)$. In particular, we introduce an intermediate system, which is the same as that

described by $Z(L_x)$ but with all segments at $x = l$ experiencing a repulsive potential U_c and N_c being the total number of such segments, where $1 \leq l \leq L_x$ is an arbitrary integer due to the periodic boundary conditions. Furthermore, a bridging bond between two lattice sites at $x = l - 1$ and $l + 1$ (under the periodic boundary conditions), respectively, having the same y - (and in 3D z -) coordinate is allowed with a repulsive potential U_b and N_b being the total number of such bonds (that is, each lattice site at $x = l - 1$ and $l + 1$ has $z_L + 1$ allowed bonds in terms of chain connectivity or nearest neighbors in terms of non-bonded interactions); note that the bridging bonds do not introduce branching and chains are still linear in our model. The canonical partition function of this intermediate system is given by $Z'(U_c, U_b) = (1/n!) \sum_{\mathbf{R}} \exp[-H(\mathbf{R}) - U_c N_c(\mathbf{R}) - U_b N_b(\mathbf{R})]/W(\mathbf{R})$; note that $Z'(U_c = 0, U_b \rightarrow \infty) = Z(L_x)$ and $Z'(U_c \rightarrow \infty, U_b = 0) = Z(L_x - 1)(\rho_0!)^{-A}$.

Re-writing $Z'(U_c, U_b) = \sum_{N_c} \sum_{N_b} \Omega(N_c, N_b) \exp(-U_c N_c - U_b N_b)$ with the density of states (DoS) having N_c contacts and N_b bridging bonds given by

$$\Omega(N_c, N_b) = \frac{1}{n!} \sum_{\mathbf{R}} \delta_{N_c, N_c(\mathbf{R})} \delta_{N_b, N_b(\mathbf{R})} \frac{\exp[-H(\mathbf{R})]}{W(\mathbf{R})}, \quad (10)$$

we have

$$P(\phi) = \frac{1}{A} \ln \frac{\sum_{N_c} \Omega(N_c, N_b = 0)}{\sum_{N_b} \Omega(N_c = 0, N_b)} - \ln(\rho_0!). \quad (11)$$

While this in principle allows us to calculate pressure by estimating the 2D DoS $\Omega(N_c, N_b)$, for large systems it is difficult to obtain $\Omega(N_c, N_b)$ accurately. We therefore re-write Eq. (11) as

$$P(\phi) = \frac{1}{A} \ln \frac{\sum_{N_c} \omega^{(N_b=0)}(N_c)}{\sum_{N_b} \omega^{(N_c=0)}(N_b)} - \ln(\rho_0!) \quad (12)$$

with $\omega^{(N_b=0)}(N_c) \equiv \Omega(N_c, N_b = 0)/\Omega(N_c = 0, N_b = 0)$ and $\omega^{(N_c=0)}(N_b) \equiv \Omega(N_c = 0, N_b)/\Omega(N_c = 0, N_b = 0)$, which requires two independent simulations of bulk systems

described by $Z(L_x)$ and $Z(L_x - 1)$, respectively, to estimate the two 1D normalized DoS $\omega^{(N_b=0)}(N_c)$ and $\omega^{(N_c=0)}(N_b)$. Note that Eq. (12) is equivalent to

$$P(\phi) = \frac{1}{A} \left[\ln \frac{Z(L_x)}{Z_c(L_x - 1)} - \ln \frac{Z(L_x - 1)}{Z_c(L_x - 1)} \right], \quad (13)$$

where $Z_c(L_x - 1)$ denotes the canonical partition function of the *confined* system having $L_x - 1$ lattice layers in the x -direction between two parallel and impenetrable walls placed perpendicular to the x -direction.

2.2.2 The Double Repulsive Plane (DRP) Method

The second variant we propose is to use the *confined* system having $L_x - 2$ lattice layers in the x -direction to bridge the two bulk systems, i.e.,

$$P(\phi) = \frac{1}{A} \left[\ln \frac{Z(L_x)}{Z_c(L_x - 2)} - \ln \frac{Z(L_x - 1)}{Z_c(L_x - 2)} \right], \quad (14)$$

which can be compared with Eq. (13). To estimate the first term in the square brackets in Eq. (14), we introduce an intermediate system, which is the same as that described by $Z(L_x)$ but with all segments at $x = l$ and $l + 1$ (under periodic boundary conditions; referred to as the double repulsive plane, DRP) experiencing a repulsive potential U_c and $N_{c,2}$ being the total number of such segments, where $1 \leq l \leq L_x$ is an arbitrary integer. The canonical partition function of this intermediate system can then be re-written as $Z'(U_c) = \sum_{N_{c,2}} \Omega^{(2)}(N_{c,2}) \exp(-U_c N_{c,2})$ with DoS having $N_{c,2}$ contacts $\Omega^{(2)}(N_{c,2}) = (1/n!) \sum_{\mathbf{R}} \delta_{N_{c,2}, N_{c,2}(\mathbf{R})} \exp[-H(\mathbf{R})]/W(\mathbf{R})$. Similarly, to estimate the second term in the square brackets in Eq. (14), we introduce an intermediate system, which is the same as that described by $Z(L_x - 1)$ but with one repulsive plane, and re-write its canonical partition function as $Z'(U_c) = \sum_{N_c} \Omega(N_c) \exp(-U_c N_c)$. Eq. (14) can finally be

re-written as

$$P(\phi) = \frac{1}{A} \ln \frac{\sum_{N_{c,2}} \omega^{(2)}(N_{c,2})}{\sum_{N_c} \omega(N_c)} - \ln(\rho_0!) \quad (15)$$

with $\omega^{(2)}(N_{c,2}) \equiv \Omega^{(2)}(N_{c,2})/\Omega^{(2)}(N_{c,2} = 0)$ and $\omega(N_c) \equiv \Omega(N_c)/\Omega(N_c = 0)$, which also requires two independent simulations of bulk systems described by $Z(L_x)$ and $Z(L_x - 1)$, respectively, to estimate $\omega^{(2)}(N_{c,2})$ and $\omega(N_c)$.

2.2.3 Simulation Details

For given n , N , ρ_0 , A and ϕ , we use WL-OE sampling¹³ to estimate the above DoS in RPBB and DRP methods. The simulation procedure is similar to that described in Sec. 2.1.1. Taking the estimation of $\omega(N_c)$ as an example, we can simply replace z , n , and n_m used in Sec. 2.1.1 by ω , N_c , and $A\rho_0$, respectively. In addition, we use only nVT trial moves of random segment hopping and chain reptation²² with probabilities of 0.2 and 0.8, respectively, which have the acceptance criterion

$$\mathcal{P}_{acc}(\mathbf{R} \rightarrow \mathbf{R}') = \min \left[1, \frac{Wg(N_c)}{W'g(N'_c)} \exp(-\Delta H) \right] \quad (16)$$

instead of Eq. (6); here ΔH is the difference in H between the trial configuration \mathbf{R}' (having W' and N'_c) and the current configuration \mathbf{R} (having W and N_c), and one MCS is defined as nN trial moves. Finally, at the end of simulation step j in OE sampling, we estimate $\omega(N_c)$ as $\ln \omega_j(N_c) = \ln[h_j(N_c)/h_j(N_c = 0)] + \ln[g_j(N_c)/g_j(N_c = 0)]$. The same procedure as given here is used to estimate other DoS with N_c replaced accordingly.

2.3 Combining the Z Method with RPBB or DRP Method

We finally propose to combine the Z method, which is very efficient as shown in Sec. 3.1 below, with either RPBB or DRP method. This overcomes not only the limitation that

the Z method cannot be applied at high ϕ , but also the drawback of RPBB and DRP methods that two simulation runs are required to obtain P at a single ϕ -value. It is easy to show that

$$P(\phi) = \frac{\rho_0 \phi^2}{N} \left[\frac{\partial [F(\phi, V)/n]}{\partial \phi} \right]_n = \frac{\phi^2}{V} \left[\frac{\partial [F(\phi, V)/\phi]}{\partial \phi} \right]_V, \quad (17)$$

which leads to

$$\ln z(n, V) = -V\phi \int_{\phi_0}^{\phi} \frac{P(\varphi)}{\varphi^2} d\varphi + \frac{n}{n_m} \ln z(n_m, V) + \left(\frac{n}{n_m} - 1 \right) \ln Z_0, \quad (18)$$

where $\phi_0 = n_m N / \rho_0 V$. Eq. (18) allows the estimation of $z(n, V)$ for $n > n_m$, thus giving P over the *entire* range of $\phi \in [0, \phi'_m]$, where ϕ'_m denotes the largest polymer volume fraction used in RPBB or DRP method and can be quite close to 1 as shown in Sec. 3.3 below. In particular, our Z method at V gives $z(n_m, V)$, and either RPBB or DRP method is used to obtain $P(\varphi)$ at several $\varphi \in [\phi_0, \phi'_m]$. Cubic spline interpolation can then be used for the $P(\varphi)/\varphi^2$ data to evaluate the integral in Eq. (18) for all $n \in (n_m, n'_m]$, where $n'_m \equiv \lfloor \phi'_m \rho_0 V / N \rfloor$ with $\lfloor a \rfloor$ denoting the largest integer not greater than a . Note that, because the integral does not involve V , the box size used in RPBB or DRP method can be different from V .

3 Results and Discussions

To demonstrate our methods, here we apply them to 2D athermal polymer solutions with $N = 20$ and $\rho_0 = 1$ (thus $P = \Pi$) on the square lattice. We also split Π into the ideal part $\Pi^{id} = \rho_0 \phi / N$ (which is due to $Z^{id} = (V z_L^{N-1})^n / n!$ with $z_L = 4$) and the excess part $\Pi^{ex} = \Pi - \Pi^{id}$ (which is due to $Z^{ex} \equiv Z / Z^{id}$).

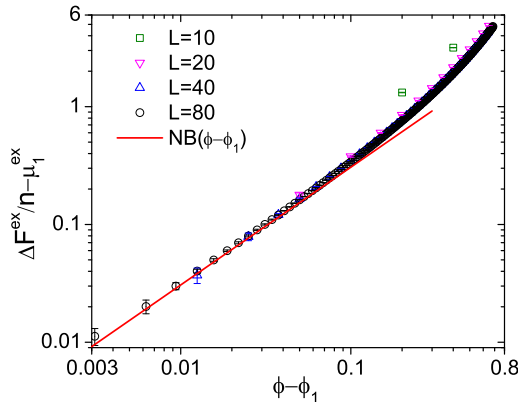


Figure 1: Logarithmic plot of $\Delta F^{ex}(n, V)/n - \mu_1^{ex}$ vs. $\phi - \phi_1$ obtained from our Z method in various square boxes of length L . The leftmost data point at each L corresponds to $n = 2$; for $L \geq N$, our simulations give $\Delta F^{ex}(n = 1, V) = \mu_1^{ex}$ within the sampling error. See main text for details.

3.1 The Z Method

Fig. 1 shows $\Delta F^{ex}(n, V)/n - \mu_1^{ex}$ as a function of $\phi - \phi_1$ obtained from our estimated $z(n, V)$ in various square boxes of length $L = \sqrt{V}$, where $\Delta F^{ex}(n, V) \equiv F^{ex}(n, V) - F^{ex}(n = 0, V)$ with the excess Helmholtz free energy $F^{ex}(n, V) = -\ln Z^{ex}(n, V)$, the exact value of the excess chemical potential of a single chain $\mu_1^{ex} = -\ln(83,779,155/z_L^{N-2})$ is obtained via enumeration of single-chain configurations in a square box of $L \geq N$ (where the numerator is the number of allowed configurations of the chain with the position of its first segment and the orientation of its first bond fixed), and $\phi_1 \equiv N/\rho_0 V$. For $\phi \lesssim 0.01$, our data are consistent with the expected result of $\Delta F^{ex}(n, V)/n - \mu_1^{ex} = (NB/\rho_0)(\phi - \phi_1)$ explained below.

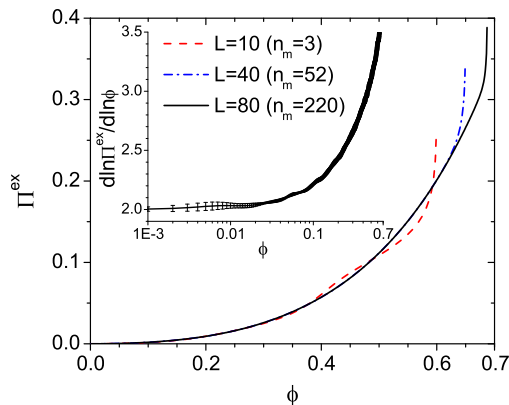


Figure 2: $\Pi^{ex}(\phi)$ obtained from our Z method in various boxes of length L . The inset shows a semi-logarithmic plot of $d \ln \Pi^{ex} / d \ln \phi$ vs. ϕ obtained at $L = 80$. See main text for details.

With our estimated $z(n, V)$, $\Pi^{ex}(\phi)$ is then obtained from Eqs. (4) and (5) and is shown in Fig. 2. We first note that the inset of Fig. 2 shows $d \ln \Pi^{ex} / d \ln \phi$ obtained at $L = 80$, which clearly gives $\Pi^{ex} = B\phi^2$ for $\phi \lesssim 0.01$; unweighted linear least-squares regression of our $\Pi^{ex}(\phi)$ data in this region gives the second virial coefficient (or the excluded-volume parameter) $B = 0.153 \pm 0.003$. From $\Pi^{ex} = -(\partial \Delta F^{ex} / \partial V)_n$, one finds $\Delta F^{ex} / n - \mu_1^{ex} = (N / \rho_0) \int_{\phi_1}^{\phi} (\Pi^{ex} / \phi^2) d\phi$; at small ϕ , $\Pi^{ex} = B\phi^2$ therefore gives $\Delta F^{ex}(n, V) / n - \mu_1^{ex} = (NB / \rho_0)(\phi - \phi_1)$ shown in Fig. 1.

Fig. 2 shows that our $\Pi^{ex}(\phi)$ data have negligible finite-size effects (FSE) when $L \geq N$, except near the largest ϕ -value. The largest ϕ -value of each curve in Fig. 2 is limited by the (finite) value of n_m used in the simulation, near which $\Pi^{ex}(\phi)$ is clearly not accurate due to the cut-off in n -space. While the upper limit of n_m in a box of finite

V is given by $n_{\max} \equiv \rho_0 V/N$ (i.e., $\phi = 1$), the acceptance rate of chain insertion/deletion becomes very low at high ϕ (even with the configurational bias¹), especially for large N at $\rho_0 = 1$. Although our acceptance criteria, Eqs. (7) and (8), can expedite the sampling at high ϕ , setting n_m too close to n_{\max} makes the simulation time prohibitively long. Our Z method is therefore most efficient at low to intermediate $\phi \lesssim 0.7$. In Sec. 3.2 below, we analyze in detail the error caused by the cut-off in n -space.

Table 1 compares our $\Pi(\phi)$ data obtained at $L = 20$ and 80 with those in Ref. [10] obtained using RWM, where a box of 60×30 was used, and clearly shows that our data have no FSE (within our sampling error) and are much more accurate than those obtained using RWM. Moreover, our Z method gives Π over a range of (continuous and exact) ϕ in a single simulation run similar to HEM (note that ϕ takes discrete values at each lattice layer and has statistical error in HEM), in great contrast to at least five runs (at various λ) used in Ref. [10] to numerically estimate the integral over λ at a single ϕ -value. Our Z method further avoids the large simulation box required by LDA in HEM.^{5,18} It is therefore much more efficient than *all* the existing methods^{2-8,10,15,18} for calculating the bulk pressure at low to intermediate ϕ ($\lesssim 0.7$) on a lattice.

Even better, with $z(n, V)$ estimated, our Z method actually gives complete thermodynamics of the system as a function of ϕ . In particular, the excess chain chemical potential $\mu^{ex} \equiv (\partial F^{ex}/\partial n)_V$ can be calculated over the same range of ϕ in two different ways: (1) $\mu_{nVT}^{ex}(\phi) = F^{ex}(n, V) - F^{ex}(n-1, V)$, which is the same as obtained from Widom insertion in nVT simulations,²⁵ and (2) $\mu_{\mu VT}^{ex}(\phi)$ by solving μ from Eq. (5) and then subtracting $\mu^{id} = \ln(\rho_0 \phi/N) - (N-1) \ln z_L$ at given ϕ . The plot of $\mu_{nVT}^{ex}(\phi) - \mu_1^{ex}$ vs.

Table 1: Comparison of our $\Pi(\phi)$ data obtained from the Z method at two L -values with those from RWM reported in Ref. [10] (where an error bar of 0.0008, 0.0005, 0.0003, and 0.0003, respectively, was given for each ϕ -value from low to high).

ϕ	$\Pi (L = 20)$	$\Pi (L = 80)$	Π (Ref. [10])
0.2356	0.02564 ± 0.00001	0.02565 ± 0.00001	0.0256 ± 0.0005
0.4580	0.10813 ± 0.00009	0.10819 ± 0.00002	0.107 ± 0.001
0.5896	0.21922 ± 0.00008	0.21921 ± 0.00003	0.217 ± 0.002
0.6336	0.27428 ± 0.00021	0.27446 ± 0.00004	0.274 ± 0.003

$\phi - \phi_1$ is similar to Fig. 1 (thus not shown), except that $\mu_{nVT}^{ex}(\phi) - \mu_1^{ex} = 2(NB/\rho_0)(\phi - \phi_1)$ for $\phi \lesssim 0.01$. Fig. 3 shows FSE on μ_{nVT}^{ex} at $\phi = 0.4$; for large L , μ_{nVT}^{ex} exhibits a linear relation with L^{-2} as predicted in Ref. [26] (similar results are obtained for $\Delta F^{ex}/n$ and not shown), and linear fitting of our data at $L = 40, 60$ and 80 gives $\mu_{nVT}^{ex} = 4.78 \pm 0.01$ in the thermodynamic limit (i.e., $L \rightarrow \infty$), which is clearly different from our μ_{nVT}^{ex} obtained at finite L .

On the other hand, the plot of $\mu_{\mu VT}^{ex}(\phi) - \mu_1^{ex}$ vs. ϕ is similar to Fig. 2 (thus not shown), except that $\mu_{\mu VT}^{ex}(\phi) - \mu_1^{ex} = 2(NB/\rho_0)\phi$ for $\phi \lesssim 0.01$.²⁷ Fig. 3 further shows that our $\mu_{\mu VT}^{ex}(\phi)$ data have no FSE (within our sampling error) for $L \gtrsim N$, and is consistent with the above value in the thermodynamic limit obtained from the extrapolation of μ_{nVT}^{ex} . The same is found at other ϕ -values. $\mu_{\mu VT}^{ex}$ is therefore the preferred way to calculate μ^{ex} .

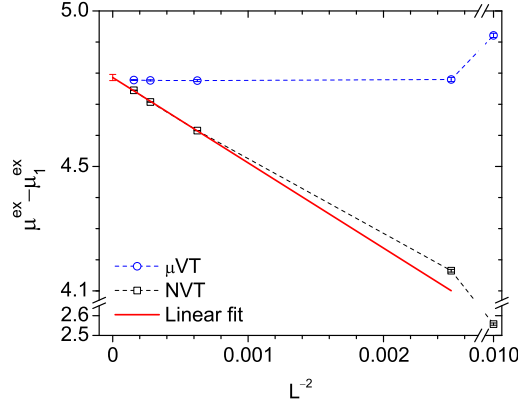


Figure 3: FSE on μ^{ex} at $\phi = 0.4$ obtained from our Z method. See main text for details.

Similarly, $d \ln \Pi^{ex} / d \ln \phi = (1/\kappa_T - \rho_0 \phi / N) / \Pi^{ex}$ shown in the inset of Fig. 2 is directly calculated from our estimated $z(n, V)$ as

$$\frac{d \ln \Pi^{ex}}{d \ln \phi} = \frac{\rho_0 \phi}{N \Pi^{ex}} \left[\frac{n_1/n_0}{n_2/n_0 - (n_1/n_0)^2} - 1 \right] \quad (19)$$

with $n_i \equiv \sum_{n=0}^{n_m} n^i \exp(\mu n) z(n, V)$ for $i = 0, 1, 2$, from which κ_T over the same range of ϕ can be obtained and also exhibits negligible FSE when $L \geq N$ as shown in Fig. 4; note that $\lim_{\phi \rightarrow 0} \kappa_T \phi / N = 1$.

Finally, we note that an analogous method of WL-OE sampling in μ -space could also be designed, which is based on the direct estimation of $\Xi(\mu, V)$ of a bulk system for a range of μ in a single simulation; Eqs. (4) and (5) then become $\Pi(\mu) = (1/V) \ln[\Xi(\mu, V)/\Xi_0]$ and $\phi(\mu) = (N/\rho_0 V)(\partial \ln \Xi / \partial \mu)_V$, respectively, also leading to $\Pi(\phi)$ over a range of ϕ . Compared to our Z method, however, this method has the drawback that μ -space is intrinsically continuous and must be discretized during the simulation, which leads to numerical error²⁸ in the calculated ϕ .

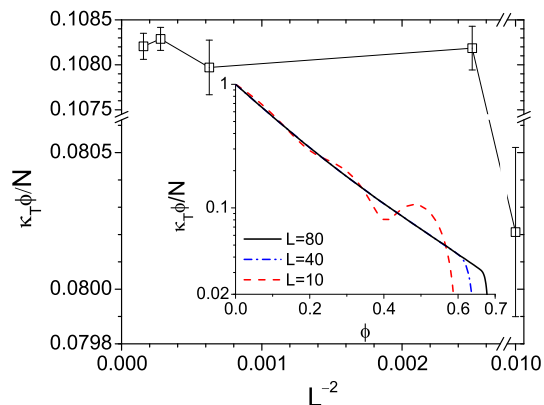


Figure 4: FSE on κ_T at $\phi = 0.4$ obtained from our Z method. The inset shows a semi-logarithmic plot of $\kappa_T(\phi)$ obtained in various boxes of length L . See main text for details.

3.2 Error Analysis due to Cut-Off in n -Space

Here we analyze in detail the error in our Z method caused by the cut-off in n -space (i.e., the use of $n_m < n_{\max}$). Denoting the exact value of Π (apart from FSE and sampling error) by

$$\Pi^*(\mu) = \frac{1}{V} \ln \sum_{n=0}^{n_{\max}} \exp(\mu n) z(n, V), \quad (20)$$

and assuming that the estimated $z(n, V)$ is not affected by the cut-off (which is justified by our acceptance criterion Eq. (5)), we find

$$[\Pi^*(\mu) - \Pi(\mu)]V = \ln \left\{ 1 + \frac{\sum_{n=n_m+1}^{n_{\max}} \exp(\mu n) z(n, V)}{\exp[\Pi(\mu)V]} \right\} > 0. \quad (21)$$

The curve of $\Pi^{ex}(\phi)$ shown in Fig. 2, however, bends upwards near the largest ϕ -value, which is actually due to the error in $\phi(\mu)$ caused by the cut-off.

We therefore denote the exact value of ϕ (apart from FSE and sampling error)

by

$$\phi^*(\mu) = \frac{N}{\rho_0 V} \frac{\sum_{n=0}^{n_{\max}} n \exp(\mu n) z(n, V)}{\sum_{n=0}^{n_{\max}} \exp(\mu n) z(n, V)}. \quad (22)$$

To show that $\phi^*(\mu) > \phi(\mu)$ (or equivalently $[\sum_{n=0}^{n_m} \exp(\mu n) z(n, V)] [\sum_{n=0}^{n_{\max}} n \exp(\mu n) z(n, V)] > [\sum_{n=0}^{n_m} n \exp(\mu n) z(n, V)] [\sum_{n=0}^{n_{\max}} \exp(\mu n) z(n, V)]$), we note that

$$\left[\sum_{n=0}^{n_m} e^{\mu n} z(n, V) \right] \left[\sum_{n=n_m+1}^{n_{\max}} n e^{\mu n} z(n, V) \right] > \left[\sum_{n=0}^{n_m} n e^{\mu n} z(n, V) \right] \left[\sum_{n=n_m+1}^{n_{\max}} e^{\mu n} z(n, V) \right]. \quad (23)$$

Estimating the error then amounts to finding an upper bound of $\Pi^*(\mu)$ and $\phi^*(\mu)$, respectively. For this purpose, we note that $\ln z(n, V)$ is a concave function with varying n (i.e., $(\partial^2 \ln z / \partial n^2)_V < 0$), as can be seen from Fig. 1 and the inset of Fig. 8 below; its upper bound for $n \in [n_m + 1, n_{\max}]$ can then be taken as $\ln \bar{z}(n, V) = (\partial \ln z / \partial n)_V|_{n=n_m} (n - n_m) + \ln z(n_m, V)$, where $(\partial \ln z / \partial n)_V|_{n=n_m} = (3/2) \ln z(n_m, V) - 2 \ln z(n_m - 1, V) + (1/2) \ln z(n_m - 2, V)$ is estimated by the second-order finite difference. The upper bound of $\Pi^*(\mu)$ can therefore be taken as

$$\bar{\Pi}(\mu) = \frac{1}{V} \ln \left[\sum_{n=0}^{n_m} \exp(\mu n) z(n, V) + \sum_{n=n_m+1}^{n_{\max}} \exp(\mu n) \bar{z}(n, V) \right], \quad (24)$$

and that of $\phi^*(\mu)$ can be taken as

$$\bar{\phi}(\mu) = \frac{N}{\rho_0 V} \frac{\sum_{n=0}^{n_m} n \exp(\mu n) z(n, V) + \sum_{n=n_m+1}^{n_{\max}} n \exp(\mu n) \bar{z}(n, V)}{\sum_{n=0}^{n_m} \exp(\mu n) z(n, V) + \sum_{n=n_m+1}^{n_{\max}} \exp(\mu n) \bar{z}(n, V)}. \quad (25)$$

To show that $\bar{\phi}(\mu) > \phi^*(\mu)$, we note that

$$\begin{aligned} & \left[\sum_{n=0}^{n_m} n e^{\mu n} z(n, V) + \sum_{n'=n_m+1}^{n_{\max}} n' e^{\mu n'} \bar{z}(n', V) \right] \left[\sum_{n=0}^{n_m} e^{\mu n} z(n, V) + \sum_{n'=n_m+1}^{n_{\max}} e^{\mu n'} z(n', V) \right] \\ & - \left[\sum_{n=0}^{n_m} e^{\mu n} z(n, V) + \sum_{n'=n_m+1}^{n_{\max}} e^{\mu n'} \bar{z}(n', V) \right] \left[\sum_{n=0}^{n_m} n e^{\mu n} z(n, V) + \sum_{n'=n_m+1}^{n_{\max}} n' e^{\mu n'} z(n', V) \right] \\ & = \sum_{n=0}^{n_m} \sum_{n'=n_m+1}^{n_{\max}} (n' - n) [\bar{z}(n', V) - z(n', V)] z(n, V) e^{\mu n} e^{\mu n'} > 0. \end{aligned} \quad (26)$$

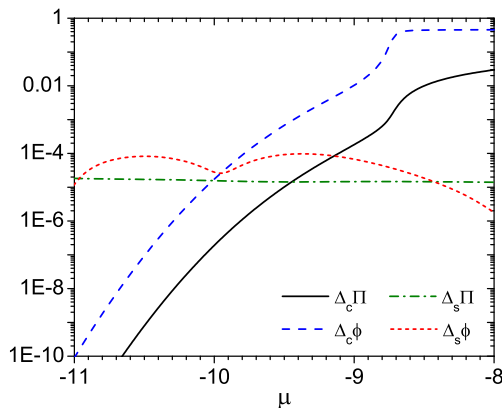


Figure 5: Comparisons of the estimated relative errors in Π and in ϕ due to the cut-off in n -space, $\Delta_c \Pi(\mu)$ and $\Delta_c \phi(\mu)$, respectively, with those due to the sampling, $\Delta_s \Pi(\mu)$ and $\Delta_s \phi(\mu)$, in our Z method for the case of $L = 80$ shown in Fig. 2.

Fig. 5 compares the estimated relative errors in Π and in ϕ due to the cut-off, $\Delta_c \Pi(\mu) \equiv \bar{\Pi}(\mu)/\Pi(\mu) - 1$ and $\Delta_c \phi(\mu) \equiv \bar{\phi}(\mu)/\phi(\mu) - 1$, with those due to the sampling, $\Delta_s \Pi(\mu)$ and $\Delta_s \phi(\mu)$ (i.e., the ratio between the standard deviation calculated from three independent WL-OE simulations and their average), respectively, for the case of $L = 80$ shown in Fig. 2. The μ -value at which $\Delta_c \Pi = \Delta_s \Pi$, denoted by μ_Π , gives the largest μ where Π is not affected by the cut-off, i.e., $\Pi(\mu) = \Pi^*(\mu)$ for $\mu < \mu_\Pi$ (within our sampling error); similarly, we have $\phi(\mu) = \phi^*(\mu)$ for $\mu < \mu_\phi$ (within our sampling error). Fig. 5 clearly shows that $\mu_\phi < \mu_\Pi$; the range of ϕ for the case of $L = 80$ shown in Fig. 2 where $\Pi^{ex}(\phi)$ is not affected by the cut-off in n -space is therefore given by μ_ϕ and corresponds to $0 \leq \phi \lesssim 0.6631$.

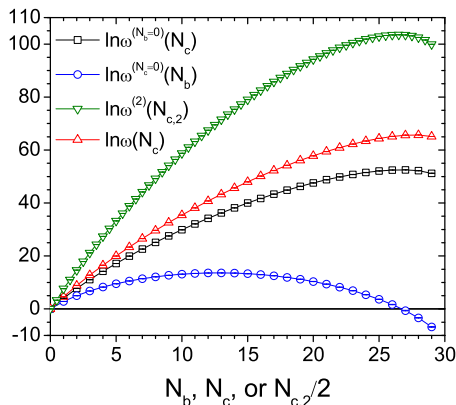


Figure 6: Normalized DoS obtained from our RPBB and DRP methods. See main text for details.

Finally, we note that this error analysis can also be applied to our combined Z and RPBB results as shown in Fig. 8 below.

3.3 RPBB and DRP Methods

Figure 6 shows the normalized DoS obtained from our WL-OE sampling with $n = 38$ and $L = 29$. We see that all DoS exhibits a maximum. Note that $\omega^{(N_b=0)}(N_c)$ is smaller than $\omega(N_c)$ for all $N_c > 0$ because the latter system has $L - 1$ instead of L lattice layers in the x -direction (thus a slightly higher polymer volume fraction). With these DoS, $P(\phi = 80/87 \approx 0.9195)$ is estimated to be 1.3239 ± 0.0011 and 1.3240 ± 0.0007 using RPBB and DRP methods, respectively, which are consistent with each other as expected.

Figure 7 shows FSE in both methods. Since n must be an integer, we judiciously choose several $\{n, L\}$ -values that give $\phi = nN/L(L - 1/2) = 80/87$. We see negligible

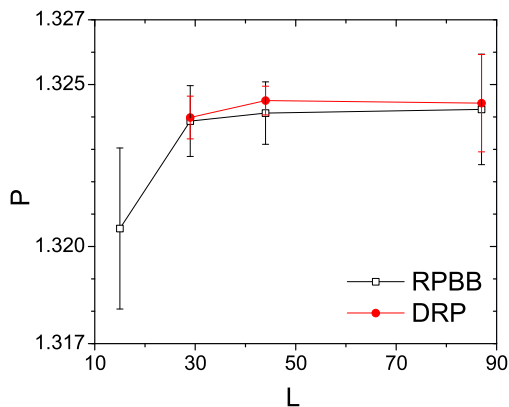


Figure 7: The bulk pressure P at $\phi = 80/87$ obtained in boxes of length $L = 15, 29, 44$ and 87 .

FSE (within our sampling error) for $L \gtrsim N$ in both methods. Note that DRP requires $\phi'_m < (L - 2)/(L - 1/2)$ and therefore cannot be used for the smallest box in Fig. 7. In comparison, RPBB requires $\phi'_m < (L - 1)/(L - 1/2)$ and makes the sampling easier (i.e., its DoS have much smaller variation than those in DRP as shown in Fig. 6).

Finally, Table 2 compares P obtained from RWM,¹⁰ RPBB and DRP methods, and shows that our methods give much more accurate results for the bulk pressure with much less computational effort. Table 2 also lists P obtained from our Z method in Sec. 3.1, which is very efficient at low to intermediate ϕ but does not work for $\phi \gtrsim 0.7$ (with $N = 20$ and $\rho_0 = 1$) where the chain insertion/deletion become inefficient.

Table 2: Comparison of P obtained from various methods. The data from Ref. [10] are at $\phi_m = 0.5896 \pm 0.0003$ and 0.8951 ± 0.0005 , respectively, where a box of 60×30 was used.¹⁰ $L = 38$ and 33 are used at $\phi = 56/95 \approx 0.5895$ and $128/143 \approx 0.8951$, respectively, in our RPBB and DRP methods. $L = 80$ and 40 are used, respectively, in our Z method and RPBB method when combined with the Z method.

P	$\phi = 56/95$	$\phi = 128/143$
Ref. [10]	0.2170 ± 0.0021	1.110 ± 0.022
RPBB method	0.2189 ± 0.0006	1.117 ± 0.001
DRP method	0.2190 ± 0.0003	1.116 ± 0.001
The Z method	0.21921 ± 0.00003	–
Z +RPBB method	0.21921 ± 0.00003	1.116 ± 0.001

3.4 The Z +RPBB Method

As RPBB method works better than DRP method, here we combine the Z method with RPBB method (denoted by Z +RPBB). The inset of Fig. 8 shows $\ln z(n, V)$ vs. n at $V = 80^2$; for $n \leq n_m = 220$ it is obtained from our Z method, and for $n > n_m$ from our Z +RPBB method, where we performed several simulations with different $n \in [54, 72]$ in a box of length $L = 40$ using RPBB method. We see that, while $z(n, V)$ obtained from our Z method monotonically increases with increasing n , it exhibits a maximum at larger n ($= 261$) as expected.

With $z(n, V)$ estimated up to $n'_m = 291$ by our Z +RPBB method, we can obtain complete

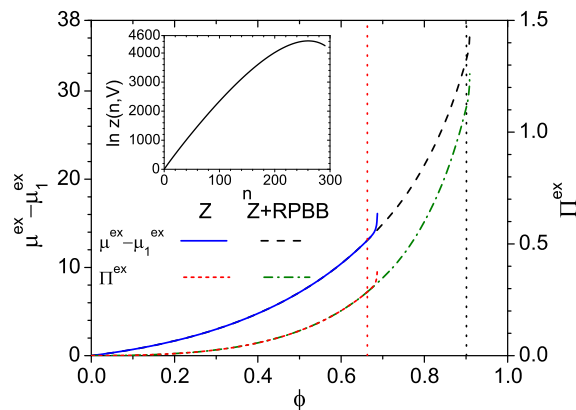


Figure 8: $\Pi^{ex}(\phi)$ and $\mu^{ex}(\phi)$ obtained from our Z and $Z+RPBB$ methods, where the two vertical lines mark the ϕ -value (0.6631 for the Z method and 0.9009 for the $Z+RPBB$ method) below which the results are not affected by the cut-off in n -space. The inset shows $\ln z(n, V)$ vs. n at $V = 80^2$; see main text for details.

thermodynamics over the entire range of continuous and exact ϕ -values. Fig. 8 shows, for example, $\Pi^{ex}(\phi)$ and $\mu^{ex}(\phi)$ calculated from Eqs. (4) and (5). We see that, for both Π^{ex} and μ^{ex} , the range extended by our $Z+RPBB$ method is more than that obtained by our Z method alone. Table 2 further compares P obtained from our $Z+RPBB$ method with those from other methods, and shows that our $Z+RPBB$ method has advantages of both the Z and RPBB/DRP methods (i.e., high accuracy and applicability to high ϕ , respectively). Finally, our $Z+RPBB$ results in the extended high- ϕ region have negligible FSE, as demonstrated in Sec. 3.1. Our $Z+RPBB$ method therefore provides, for example, a much better way of calculating μ at high ϕ than any method using chain insertion/deletion.

4 Summary

To summarize, we have proposed several novel methods for calculating the bulk pressure P in polymer lattice Monte Carlo simulations. Firstly, our Z method combines chain insertion/deletion with Wang-Landau – Optimized Ensemble sampling¹³ in the space of number of chains n to directly estimate the canonical partition function $Z(n, V)$ for a range of n (where V denotes the system volume), and is very efficient and accurate at low to intermediate polymer volume fractions ϕ (e.g., $\lesssim 0.7$). It gives not only P but also complete thermodynamics (e.g., the chain chemical potential and the isothermal compressibility) over a range of *continuous and exact* ϕ -values in a single simulation with negligible finite-size effects. Our Z method avoids the computationally expensive numerical integration required in the test-chain insertion thermodynamic integration method,^{2,5} the compressibility route,^{3,8} and the repulsive wall method (RWM),¹⁰ as well as the large box size and limitations due to the use of the external field in the hydrostatic equilibrium method,^{5,18} thus superior to *all* the existing methods^{2-8,10,15,18} for calculating P at low to intermediate ϕ on a lattice.

Secondly, our repulsive plane with bridging bonds (RPBB) and double repulsive plane (DRP) methods efficiently and accurately calculate P in canonical-ensemble simulations at high ϕ where chain insertion/deletion become inefficient. They avoid the confinement effects, the numerical integration, and the statistical error in the calculated polymer volume fraction ϕ_m in the original RWM. Finally, our combined Z and RPBB or DRP method overcomes not only the limitation that the Z method cannot be applied at high ϕ , but also the drawback of RPBB and DRP methods that two simulation

runs are required to obtain P at a single ϕ -value. It gives complete thermodynamics over the *entire* range of continuous and exact ϕ -values with negligible finite-size effects.

We have also analyzed in detail the error caused by the cut-off in n -space in the Z and the combined methods. While we have demonstrated the application and advantages of our methods using 2D athermal polymer solutions with the self- and mutual-avoiding walk on the square lattice as a simple example, it is straightforward to apply them to lattice simulations of various polymeric systems.

Acknowledgement

QW thanks Prof. Fernando Escobedo for helpful discussion and for pointing out Ref. [19] to us after our work is completed. This work was supported by NSF CAREER Award CBET-0847016, which is gratefully acknowledged.

References

- [1] Chap. 13.2.2 in D. Frenkel and B. Smit, *Understanding Molecular Simulation: From Algorithms to Applications*, 2nd ed.; Academic Press: New York, 2002.
- [2] H. Okamoto, *J. Chem. Phys.* **64**, 2686 (1976).
- [3] M. Stukan, V. Ivanov, M. Muller, W. Paul, and K. Binder, *J. Chem. Phys.* **117**, 9934 (2002).
- [4] W. Jiang and Y. Wang, *J. Chem. Phys.* **121**, 3905 (2004).
- [5] V. Ivanov, E. An, L. Spirin, M. Stukan, M. Muller, W. Paul, and K. Binder, *Phys. Rev. E* **121**, 026702 (2007).
- [6] A. D. Mackie, A. Z. Panagiotopoulos, D. Frenkel, and S. K. Kumar, *Europhys. Lett.* **27**, 549 (1994).
- [7] A. D. Mackie, A. Z. Panagiotopoulos, and S. K. Kumar, *J. Chem. Phys.* **102**, 1014 (1995).
- [8] A. Pelissetto, *J. Chem. Phys.* **129**, 044901 (2008).
- [9] A. Ferrenberg and R. Swendsen, *Phys. Rev. Lett.* **63**, 1195 (1989).
- [10] R. Dickman, *J. Chem. Phys.* **87**, 2246 (1987).
- [11] P. Zhang, B. Li, and Q. Wang, *Macromolecules* **45**, 2537 (2012).
- [12] J. Jimenez and R. Rajagopalan, *Eur. Phys. J. B.* **5**, 237 (1998).

- [13] S. Trebst, D. Huse, and M. Troyer, Phys. Rev. E **70**, 046701 (2004).
- [14] P. Zhang and Q. Wang, J. Chem. Phys. **140**, 044904 (2014).
- [15] E. Nies and P. Cifra, Macromolecules **27**, 6033 (1994).
- [16] Q. Wang, J. Chem. Phys. **131**, 234903 (2009).
- [17] T. Biben, J.-P. Hansen, and J.-L. Barrat, J. Chem. Phys. **98**, 7330 (1993).
- [18] C. Addison, J.-P. Hansen, and A. Louis, ChemPhysChem **6**, 1760 (2005).
- [19] G. Ganzenmüllera and P. J. Camp, J. Chem. Phys. **127**, 154504 (2007).
- [20] Q. Yan and J. de Pablo, Phys. Rev. Lett. **90**, 035701 (2003).
- [21] B. Schultz, K. Binder, M. Muller, and D. Landau, Phys. Rev. E **67**, 067102 (2003).
- [22] The configurational-bias Monte Carlo technique¹ can certainly be used to improve the sampling efficiency. At very high ϕ , one can use the vacancy diffusion algorithm,²³ which is more efficient than segment hopping and chain reptation; we recently generalized this algorithm to the case of $\rho_0 > 1$.²⁴
- [23] J. Reiter, T. Edling, and T. Pakula, J. Chem. Phys. **93**, 837 (1990).
- [24] P. Zhang and Q. Wang, J. Phys. Chem. B **118**, 12059 (2014).
- [25] B. Widom, J. Chem. Phys. **39**, 2808 (1963).
- [26] J. Siepmann, I. McDonald, and D. Frenkel, J. Phys.: Condens. Matter **4**, 679 (1992).

- [27] In the limit of $\phi \rightarrow 0$, we have $\exp(\mu) \rightarrow 0$ and thus $\phi(\mu) = (N/\rho_0 V) \exp(\mu) Z(n = 1, V)/Z_0$, from which one finds $\mu^{ex} = F^{ex}(n = 1, V) - F^{ex}(n = 0, V) = \mu_1^{ex}$.
- [28] M. Kobrak, J. Comput. Chem. **24**, 1437 (2003).